ACS OMEGA

http://pubs.acs.org/journal/acsodf

Article

Refractive Indexes and Spectroscopic Properties to Design Er^{3+}-Doped SiO_2–Ta_2O_5 Films as Multifunctional Planar Waveguide Platforms for Optical Sensors and Amplifiers

Jefferson L. Ferrari, Karmel de O. Lima, and Rogéria R. Gonçalves*

Cite This: *ACS Omega* 2021, 6, 8784–8796

Read Online

ACCESS | Metrics & More | Article Recommendations

ABSTRACT: This paper reports on the news about refractive index measurements and spectroscopic features of thin films, which can be applied as optical planar waveguides, focusing on their manufacturing processes, designs, and possible applications as optical amplifiers and sensors. Er^{3+}-doped SiO_2–Ta_2O_5 planar waveguides, with Si/Ta ratios of 90:10, 80:20, 70:30, 60:40, and 50:50, were prepared by a soft sol–gel process. Multilayer films were deposited by the dip-coating technique onto 10 μm SiO_2–Si (100) p-type silicon and Si (100) silicon easily and successfully. The mechanisms of the densification process, porosity, and hydroxy group or water molecule occurrence have been accompanied by m-line and vibrational spectroscopy analyses. The thickness and refractive index values were used to understand better the influence of temperature and annealing time on the densification of the bulk films and the reduction of the pore volume as the tantalum oxide concentration increases. The refractive index shows the density of the films, and by the atomic force microscopy (AFM) technique, the films showed low surface roughness, achieving relatively high light confinement within the waveguide structure, and negligible optical loss due to surface scattering. Nanoparticle crystallization of Ta_2O_5 with size distribution ranging from 2.0 to 15.0 nm embedded in SiO_2 was observed with size depending on annealing time and tantalum concentration. Intense and broadband emission positioned at 1550 nm, which is attributed to the $^4I_{13/2} \rightarrow {}^4I_{15/2}$ transition of Er^{3+} ions, was observed for all planar waveguides under excitation at 271, 272, and 278 nm. Depending on the porosity degree, the adsorption of H_2O molecules occurs, changing the refractive index and contributing to the deactivation of excited states of Er^{3+} ions, making them an optical platform for use as an optical sensor for different species. Besides, the densified waveguides containing 20 or 30 mol % Ta exhibit high potential for applications as broadband optical amplifiers for wavelength division multiplexing (WDM), optical sensing, or augmented reality.

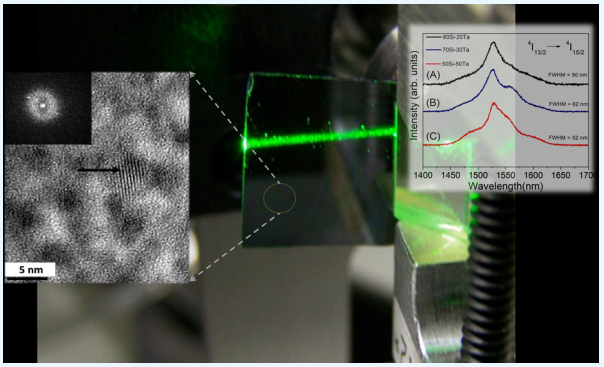

1. INTRODUCTION

Recent modern applications in the field of photonics have involved the use of waveguides. In the past years, new optical devices have been created enabling greater performance, more affordable prices for mass production, or even the development of new technologies. The relentless pursuit for new devices with high performance has led to a significant increase in research considering strategic areas as health, environment, and telecommunication. Planar waveguides have emerged as a target of many research groups and optoelectronic industries in the world and have been used as a platform for optical information transport in integrated optical devices.[1] For instance, their use as a platform for optical sensors is one of the great potential applications for waveguides.[2−5] Nowadays, most of the wearable augmented reality display devices operate using waveguide technology, of which some are commercial products. However, mass production has been already limited by cost and performance in many cases.[6] Among the different planar waveguide applications, the different highlights are due to the demand for information through visual means, and the augmented reality created through special glasses has been presenting a special need.[7−9] This type of application of planar waveguides regarding augmented reality manages to bring, in virtual ways, environments that in most cases would be impossible to visit in person. Thus, the contribution to the development of knowledge based on real facts becomes indispensable and possible to achieve without leaving home, for example.

Received: November 2, 2020
Accepted: February 5, 2021
Published: March 25, 2021

https://doi.org/10.1021/acsomega.0c05351
ACS Omega 2021, 6, 8784–8796

Among the materials used to manufacture optical devices as planar waveguides, those based on SiO_2 have been highlighted due to physical, mechanical, and chemical properties.[10] For instance, one of the most studied silica-based systems and commercial products found in the market is the Er^{3+}-doped optical fiber amplifier (EDFA), which contains low rare-earth (RE^{3+}) ion concentration to achieve enough gain.[11−13] However, the RE^{3+} concentration must be increased by at least 2 orders of magnitude than its counterpart Er^{3+}-doped planar waveguide amplifier (EDWA). A high RE^{3+} ion concentration leads to the formation of clusters in the silica-based system, and consequently, competitive processes such as energy migration between them, energy transfer, and upconversion can occur, reducing drastically the near-infrared (NIR) luminescence quantum yield. The choice of the host to have great optical, structural, morphological, and luminescence properties is undoubtedly one of the most critical factors for the development of photonic devices. Regarding silicate-based planar waveguides, binary oxides, like SiO_2−MO_2 (M = Hf, Zr, and Ti),[14−19] have been studied and interesting optical features have been observed when doped with Er^{3+} ions. The addition of metal oxides such as Hf, Zr, and Ti to the silica host promotes refractive index tailoring, which is important to control optical parameters regarding waveguide applications and induce controlled-phase separation with a high distribution of RE^{3+} in the crystalline or amorphous metal oxide microenvironment. Luminescence at 1.5 μm has been obtained from SiO_2−MO_2 (M = Hf, Zr, Ti), and a full-width at half-maximum (FWHM) of up to 48 nm has been obtained for the amorphous system with a drastic reduction as the glass ceramic is produced. For instance, a FWHM of about 30 nm has been observed from the glass ceramic containing Er^{3+}-doped HfO_2 nanocrystals and 14 nm for that containing Er^{3+}-doped ZrO_2 nanocrystals.[19]

In previous works, we have reported outstanding unusual broadened emission in the silicate glass ceramic host, when Er^{3+}-doped Ta_2O_5 or Nb_2O_5 nanocrystals are embedded into the silica-based host, similar to that observed for tellurite glasses, the most cited host in the literature displaying large inhomogeneous broadening at 1.5 μm.[20−23]

Among several techniques used for optical material preparation, the sol−gel process followed by dip-coating deposition has been used as one of the cheapest and most versatile routes for manufacturing films that exhibit high-quality optical properties.[24] Sol−gel-prepared waveguides bring interesting solutions concerning their production because of its low cost, flexibility concerning composition, and refractive index tailoring and can be applied in a wide-ranging device geometry.[25] Besides, the precursors are homogeneously mixed at the molecular level, allowing a wide range of composition, including multicomponents, wherein some of them cannot be obtained by other methodologies. For instance, binary SiO_2−Ta_2O_5 and SiO_2−Nb_2O_5 glasses as well as the respective glass ceramics cannot be obtained by a traditional method for producing glasses through a melt−quenching process, except using a sol−gel process.[20−23] The sol−gel process usually is applied for obtaining products at room temperature or lower temperatures in comparison with other fabrication routes. The xerogels obtained by this process can be submitted to thermal annealing for elimination of undesired species such as O−H and C−H groups and H_2O molecules besides pores. Full elimination of residual species is required since they act in deactivating the excited states of RE^{3+} ions, reducing the emission quantum efficiency, and quenching the photoluminescence. Consequently, concerning sol−gel photonic materials, the densification of the host and total elimination of residual organic and hydroxyl groups represent one of the most important aims to be achieved for luminescence improvement and active planar waveguide fabrication. However, the presence of pores allows the adsorption of small molecules like water, ammonia, carbon dioxide, methanol, and others.

An understanding of the whole preparation process until the achievement of fully densified films passing through porous precursors is the aim of this work. In this sense, this work reports on how to design active or passive planar waveguides, as well as porous waveguides, which can be used as optical sensor platforms, using optical and spectroscopic parameters. The Er^{3+}-doped SiO_2−Ta_2O_5 planar waveguide samples, by changing the Si/Ta ratios as 90:10, 80:20, 70:30, 60:40, and 50:50, were prepared by the sol−gel process. Ta_2O_5 shows interesting properties regarding planar waveguide manufacturing and optoelectronic devices due to its transparency in from the near-UV (λ > 300 nm) to the infrared region along with its chemical and mechanical stability and high refractive index. Therefore, the addition of Ta_2O_5 nanocrystals to the silica matrix tailors a wide range of properties, such as refractive index, band gap energy, mechanical properties, chemical reactivity or stability, and luminescence. The latter occurs in the presence of rare-earth ions.

Here, the optical and spectroscopic properties of low loss Er^{3+}-activated planar waveguides are discussed in terms of the composition and structural properties by changing the tantalum content and thermal annealing conditions. The luminescence from RE^{3+}-doped orthorhombic Ta_2O_5-based nanocomposites opened the possibility of thin film preparation for use as active planar optical amplifiers operating not only in the C band but also in the S band and L band of telecommunication, or to be applied as optical sensors.

2. EXPERIMENTAL PROCEDURE

The Er^{3+}-doped SiO_2−Ta_2O_5 thin films, containing 0.3 mol % Er^{3+} ions, were prepared by the sol−gel route and deposited onto 10 μm SiO_2−Si (100) p-type silicon and Si (100) silicon as substrates by the dip-coating technique. Solutions with a total concentration of Si + Ta = 0.445 mol L^{-1} were obtained with Si/Ta molar ratios of 90:10, 80:20, 70:30, 60:40, and 50:50. Tantalum ethoxide and tetraethylorthosilicate (TEOS) were used as Ta and Si precursors, respectively. The preparation of a solution was based on the experimental procedure reported by Ferrari et al.;[26−28] Er^{3+} ions (0.3 mol % Er^{3+} ions in relation to the Si + Ta ions) were added from their standardized stock ethanolic solutions, which were obtained by dissolving Er_2O_3 in 0.1 mol L^{-1} HCl aqueous solution, followed by solvent exchange with ethanol. A mixture of TEOS, anhydrous ethanol, and concentrated hydrochloric acid (solution 1) was first prepared. The TEOS/HCl molar ratio was 50:1. Tantalum ethoxide, 2-ethoxyethanol, and Er^{3+} ions (solution 2) were mixed in a separate container. Then, solutions 1 and 2 were mixed and kept under stirring at room temperature for 30 min. Next, an aqueous hydrochloric acid solution (0.27 mol L^{-1}) was added to the final solution at a TEOS/HCl ratio of 1:0.007. Subsequently, the solution was filtered through a 0.2 μm filter and left to stand for 16 h for film deposition. Multiple layers were deposited by the dip-coating technique with a dipping rate of 30 mm min^{-1}.

https://doi.org/10.1021/acsomega.0c05351
ACS Omega 2021, 6, 8784−8796

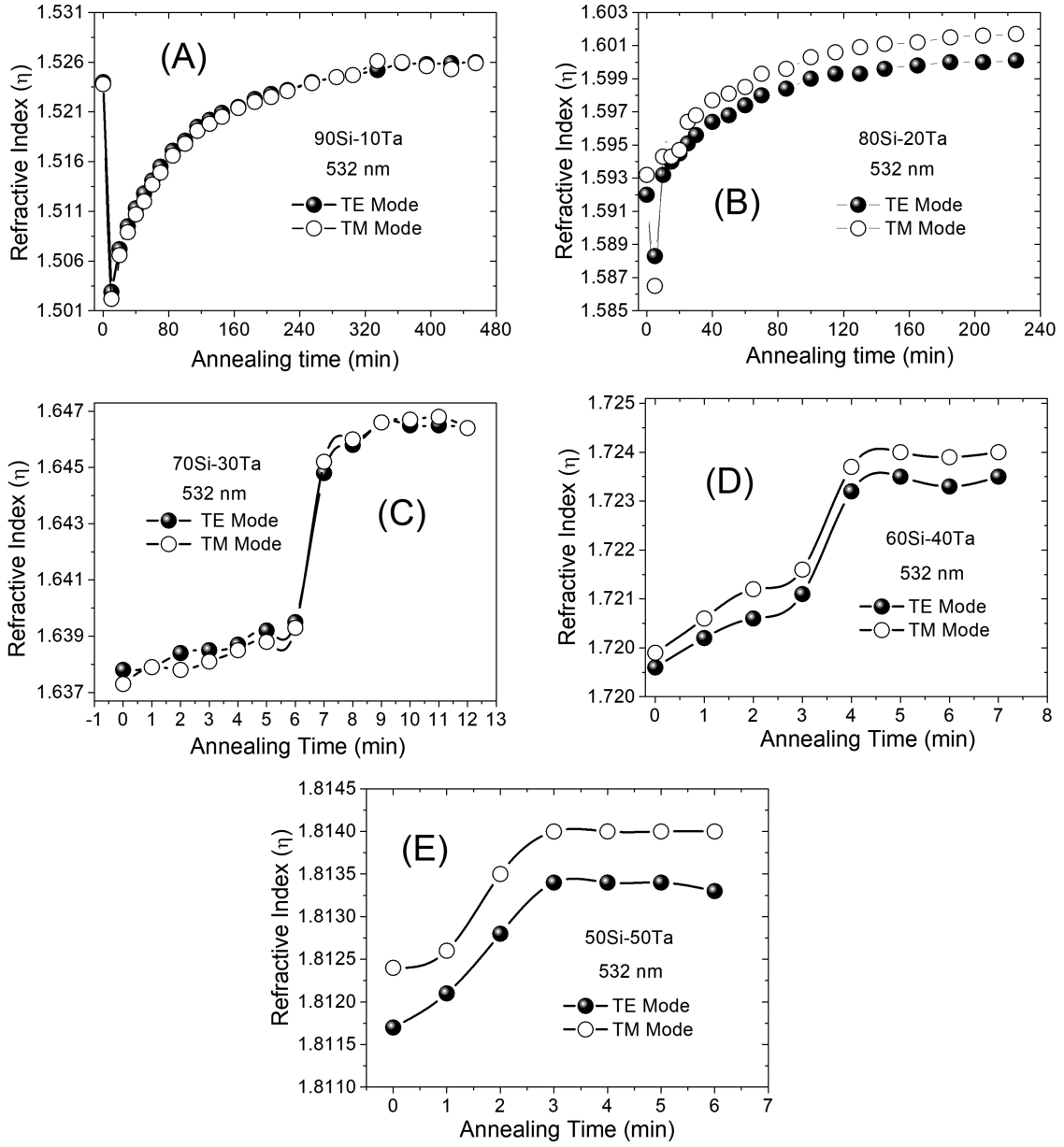

Figure 1. Refractive index values as a function of the annealing time at 900 °C of the Er^{3+}-doped planar waveguides deposited onto the 10 μm SiO_2−Si (100) p-type silicon substrate with Si/Ta ratios of (A) 90:10, (B) 80:20, (C) 70:30, (D) 60:40, and (E) 50:50.

Between each deposited layer, the film was heated to 900 °C for 60 s to ensure adhesion on the surface, organic residue elimination, and densification until 50 layers were achieved.

The planar waveguide deposited onto Si (100) silicon substrate was used to obtain information about structural properties by Fourier transform infrared (FTIR) spectra. Before further coating, each layer was annealed in an oven in air for 60 s at 900 °C. The densification process was monitored by studying the optical properties of the 50-layer films annealed at different times at the same temperature. Between each annealing time, the films deposited on the SiO_2/Si substrate were characterized by an m-line apparatus (Metricon Model 2010) by the prism coupling technique. The refractive indexes of the planar waveguides were measured at room temperature for both transverse electric (TE) and magnetic (TM) polarizations. A prism with a refractive index of 1.9644 at 632.8 nm was used. The apparatus is equipped with detectors to collect visible and near-infrared radiation. He−Ne and solid lasers, operating at 632.8 and 532 nm, respectively, and one diode laser, operating at 1538 nm, were employed.

The FTIR spectra of films deposited on the Si (100) substrate were collected in the range from 4000 to 400 cm^{-1} using a Bomem MB102 spectrometer. Finally, after full densification, the surfaces of the films were characterized by atomic force microscopy (AFM) using a Shimadzu SPM 9600 microscope operating in the contact mode. The images were collected and analyzed using SPM version 3.03 software. The high-resolution transmission electron microscopy (HRTEM) images were collected to obtain information about crystallization and phase separation using a high-resolution TEM (JEOL 3010). The film samples for HRTEM analysis were prepared with polishing ionic attacks operating GATAN-PIPS.

Emission and excitation spectra were collected at room temperature using a Jobin Yvon Fluorolog-3-Spex. The excitation and emission slits used were adjusted to give a 3 nm bandpass. The excitation spectra were collected in the

https://doi.org/10.1021/acsomega.0c05351
ACS Omega 2021, 6, 8784−8796

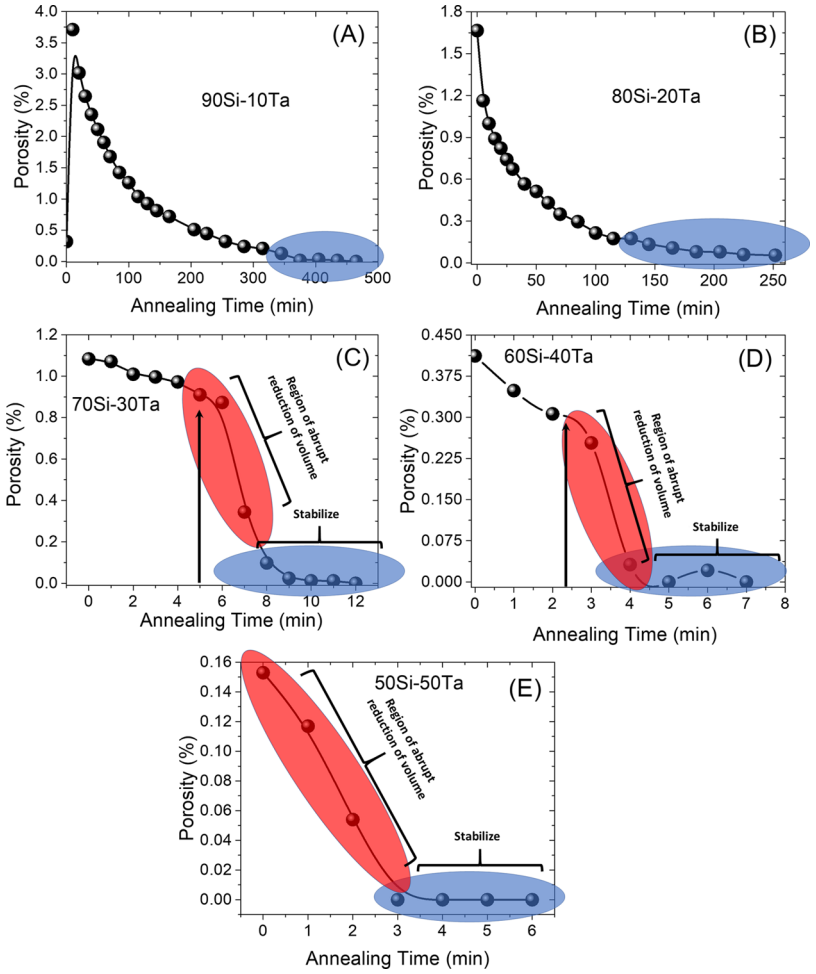

Figure 2. Porosity as a function of the annealing time at 900 °C of the Er^{3+}-doped planar waveguides deposited onto the 10 μm SiO_2−Si (100) p-type silicon substrate with Si/Ta ratios of (A) 90:10, (B) 80:20, (C) 70:30, (D) 60:40, and (E) 50:50.

region between 240 and 550 nm, with a spectral resolution of 0.2 nm and emission fixed at 1528 nm. The emission spectra were collected in the region between 1400 and 1700 nm by fixing the excitation at 271, 274, and 278 nm for samples with Si/Ta ratios of 80:20, 70:30, and 50:50, respectively.

3. RESULTS AND DISCUSSION

One of the optical parameters extremely fundamental to characterize active waveguides, mainly to calculate the light confinement coefficient, the number of the guided modes, and their effective refractive index, is the refractive index value. Furthermore, this work presents its fundamental role in the design of films that can be used as active or passive planar waveguides for integrated optics, as well as porous platforms for optical sensors for certain molecules. Through the values of the refractive indexes, the porosity of the hosts as well as their entire densification process through annealing can be closely monitored, besides their influence on rare-earth luminescence properties. Variations in optical properties of films containing different concentrations of tantalum oxide were evaluated by the m-line coupling technique.

Figure 1 shows the refractive index values at 532 and 632.8 nm for all multilayered films based on Er^{3+}-doped SiO_2−Ta_2O_5 planar waveguides after 50 layers, which were obtained as a function of annealing time. Based on the information depicted in Figure 1A,B about the films with Si/Ta molar ratios of 90:10 and 80:20, respectively, a relatively sharp change of refractive index can be observed in the first 15 min of annealing at 900 °C, reducing it significantly. This behavior indicates clear elimination of water molecules, which were distributed into or on the surface of the pores, resulting in hosts with lower refractive indexes. Before further annealing, the films are composed basically of SiO_2 and Ta_2O_5 inorganic hosts containing pores filled with H_2O molecules. As the refractive index of H_2O is around 1.333, and of air around 1.00, after H_2O elimination, the refractive index of the films decreases since air occupies the place of these species in porous structures. In this way, it can be concluded that before subsequent thermal treatment, the films exhibit pore distribution, which can adsorb water molecules. Adsorption and desorption occur reversibly, with the exposure of the film to an atmosphere containing water molecules, followed by thermal treatment at 100 °C. This temperature value is only enough to remove adsorbed water molecules, while it is not sufficient to eliminate hydroxyl groups from the pore surface of the sol−gel silicate system neither does it lead to an increase in densification.

An increase of the refractive index values occurred, which can be assigned to the elimination of the pores and densification of the host by thermal annealing at 900 °C for more than 15 min. The densification process was considered

https://doi.org/10.1021/acsomega.0c05351
ACS Omega 2021, 6, 8784−8796

Table 1. Optical Parameters Measured at 532, 632.8, and 1538 nm (TE and TM Modes) for the 0.3 mol % Er^{3+}-doped SiO_2–Ta_2O_5 Planar Waveguides before and after Full Densification at 900 °C after Different Annealing Times

	properties at 532 nm		properties at 632.8 nm		properties at 1538 nm		thickness (μm)
	TE	TM	TE	TM	TE	TM	
Before Annealing							
90Si–10Ta	2 modes n = 1.5030 (±0.0001)	2 modes n = 1.5023 (±0.0001)	2 modes n = 1.4980 (±0.0001)	2 mode n = 1.4968 (±0.0001)	1 mode n = 1.4805 (±0.0001)	1 mode n = 1.4802 (±0.0001)	~1.42
80Si–20Ta	3 modes n = 1.5883 (±0.0001)	3 modes n = 1.5865 (±0.0001)	3 modes n = 1.5805 (±0.0001)	3 modes n = 1.5814 (±0.0001)	1 mode n = 1.5609 (±0.0001)	1 mode n = 1.5623 (±0.0001)	~1.33
70Si–30Ta	6 modes n = 1.6373 (±0.0001)	6 modes n = 1.6368 (±0.0001)	5 modes n = 1.6270 (±0.0001)	5 modes n = 1.6270 (±0.0001)	2 modes n = 1.6039 (±0.0001)	2 modes n = 1.6029 (±0.0001)	~1.87
60Si–40Ta	6 modes n = 1.7201 (±0.0001)	6 modes n = 1.7204 (±0.0001)	5 modes n = 1.7077 (±0.0001)	5 modes n = 1.7080 (±0.0001)	2 modes n = 1.6799 (±0.0001)	2 modes n = 1.6791 (±0.0001)	~1.87
50Si–50Ta	8 modes n = 1.8117 (±0.0001)	8 modes n = 1.8124 (±0.0001)	6 modes n = 1.7962 (±0.0001)	6 modes n = 1.7968 (±0.0001)	2 modes n = 1.7632.8 (±0.0001)	2 modes n = 1.7624 (±0.0001)	1.84
After Different Annealing Times							
90Si–10Ta	2 modes n = 1.5260 (±0.0001)	2 modes n = 1.5254 (±0.0001)	2 modes n = 1.5202 (±0.0001)	2 modes n = 1.5201 (±0.0001)	1 mode n = 1.5035 (±0.0001)	1 mode n = 1.5038 (±0.0001)	~1.35
80Si–20Ta	3 modes n = 1.6006 (±0.0001)	3 modes n = 1.6024 (±0.0001)	3 modes n = 1.5926 (±0.0001)	3 modes n = 1.5939 (±0.0001)	1 mode n = 1.5718 (±0.0001)	1 mode n = 1.5734 (±0.0001)	~1.32
70Si–30Ta	6 modes n = 1.6461 (±0.0001)	6 modes n = 1.6461 (±0.0001)	5 modes n = 1.6358 (±0.0001)	5 modes n = 1.6361 (±0.0001)	2 modes n = 1.6122 (±0.0001)	2 modes n = 1.6122 (±0.0001)	~1.95
60Si–40Ta	6 modes n = 1.7238 (±0.0001)	6 modes n = 1.7244 (±0.0001)	5 modes n = 1.7117 (±0.0001)	5 modes n = 1.7122 (±0.0001)	2 modes n = 1.6833 (±0.0001)	2 modes n = 1.6833 (±0.0001)	~1.80
50Si–50Ta	8 modes n = 1.8133 (±0.0001)	8 modes n = 1.8140 (±0.0001)	7 modes n = 1.7980 (±0.0001)	7 modes n = 1.7986 (±0.0001)	3 modes n = 1.7632.8 (±0.0001)	3 modes n = 1.7634 (±0.0001)	~2.00

complete until achievement of constant values of the refractive index, which depends fundamentally on the tantalum content.

In Figure 1C–E, different behaviors were observed. From the first minute of annealing, an increase of the refractive index values occurred, which is correlated to the host densification process. The required time to reach full densification decreased as the tantalum oxide is added, indicating that a more cross-linked structure is successfully formed by insertion of tantalum oxide into the silica host.

The porous molar ratio also was calculated based on the refractive index for each annealing time. The presence of pores in the film for application as a planar waveguide amplifier is undesirable because they can act as light scattering centers, in accordance with the Rayleigh scattering effect, in which the intensity of scattering follows the $I = K\lambda^{-4}$ relationship, where I is the intensity of the scattering, K is the proportionality constant, and λ is the wavelength of the light. Likewise, the distribution of the pores onto the surface can adsorb water molecules, which is an efficient NIR luminescence quencher center. Based on this effect, the percentage of pores in the films for each annealing time at 900 °C was evaluated by eq 1 proposed by Yoldas et al.[29]

$$P = 1 - \left[\left(\frac{n^2 - 1}{n_d^2 - 1}\right)\left(\frac{n^2 + 1}{n_d^2 + 1}\right)100\right] \quad (1)$$

where P is the pore volume fraction, n is the refractive index of the porous film at each annealing time, and n_d is the refractive index of the film after full densification. Based on the percentage of pores calculated according to eq 1, it was possible to follow the evolution of the film densification process with the time of thermal treatment for each composition, as depicted in Figure 2. Figure 2 remarkably shows the influence of tantalum concentration on the densification process, where shorter heat treatment times are required with an increase in the amount of tantalum. The higher the tantalum concentration, the higher the densification, and the lower the annealing time required for complete pore elimination. Accordingly, it can be clearly attested that the tantalum concentration promotes a significant structural change in the silicate-derived host, allowing the preparation of a matrix with a more cross-linked structure, as observed before by us in powders of this system.[30] It is known that sol–gel silica bulks or films do not completely eliminate silanol groups after annealing at 900 °C, which is the temperature used in this work.[31] Besides, residual silanol groups have been observed by analyzing films containing 10 mol % Ta using vibrational spectroscopy,[20] which represents a problem to be circumvented for active planar waveguides for optical amplification in the near-infrared region and is advantageous to be explored as a crucial point for optical sensors for small molecules, like water molecules, in harsh environments. This is

https://doi.org/10.1021/acsomega.0c05351
ACS Omega 2021, 6, 8784–8796

because tantalum oxide has high chemical stability in acidic and basic media.

Even containing residual porosity, full densification of the host containing 10 and 20 mol % Ta has been obtained after annealing at 900 °C for 400 and 200 min, respectively. On the other hand, thermal annealing at 900 °C for 9, 4, and 3 min are enough to eliminate the presence of pores in the films containing higher tantalum contents, with the Si/Ta molar ratios of 70:30, 60:40, and 50:50, respectively. Similar behavior was observed by Zampedri et al.[17] in films based on Er^{3+}-doped SiO_2–HfO_2, where an increase of hafnium oxide amount in the binary SiO_2–HfO_2 system decreases the time needed for thermal annealing for elimination of water molecules from the pores and of hydroxyl groups from the pore surface to accomplish full densification of the planar waveguides.

The complete pore removal is extremely important for photonic materials, to be specially applied as low-loss active planar waveguides due to the reduction of scattering centers in the devices minimizing the contribution of volume scattering to the optical losses and removal of residual hydroxyl and water molecules inside the pores abolishing the luminescence quenching centers.

The refractive index, thickness, and number of propagation modes in the TE and TM polarization modes at 532, 632.8, and 1538 nm were acquired for films before and after full densification, which are summarized in Table 1.

The refractive index, number of modes, and thickness of films increase as a function of the nominal tantalum content. In accordance with Gonçalves et al.,[15,32] the refractive index of the SiO_2 films prepared by the sol–gel method is around 1.4603, and in accordance with Chaneliere et. al.,[33] the refractive index of Ta_2O_5 films is between 1.93 and 2.15, which is dependent on the synthesis method. Therefore, it is expected an increase of the refractive indexes as the tantalum oxide content is added to the silica host, corroborating with the measurements.

The theoretical refractive indexes of Ta_2O_5 and SiO_2 used to calculate the refractive index of the binary composition material were 2.1852 and 1.4603 (at 532 nm), respectively. Lorentz–Lorenz and linear equations were used to calculate the theoretical value of the refractive index of each SiO_2–Ta_2O_5 binary system. The Lorentz–Lorenz equation is represented in eq 2 and likewise reported by Rocha et al.[34] and Aquino et al.[35]

$$\frac{n^2-1}{n^2+2} = f_{SiO_2}\frac{n_{SiO_2}^2-1}{n_{SiO_2}^2+2} + f_{Ta_2O_5}\frac{n_{Ta_2O_5}^2-1}{n_{Ta_2O_5}^2+2} \quad (2)$$

Eq 1 can be rearranged as follows

$$n = \sqrt{\frac{(2A+1)}{(1-A)}} \quad (3)$$

where A can be written as

$$A = f_{SiO_2}\frac{n_{SiO_2}^2-1}{n_{SiO_2}^2+2} + f_{Ta_2O_5}\frac{n_{Ta_2O_5}^2-1}{n_{Ta_2O_5}^2+2} \quad (4)$$

The linear equation (eq 5) is represented as follows

$$n = f_{SiO_2}n_{SiO_2} + f_{Ta_2O_5}n_{Ta_2O_5} \quad (5)$$

where n is the refractive index, f_{SiO_2} and $f_{Ta_2O_5}$ are the molar fractions of each component, and n_{SiO_2} and $n_{Ta_2O_5}$ are the refractive indexes of each component.

The refractive index values of the fully densified films are in good agreement with the theoretical values obtained by the Lorentz–Lorenz equation, as can be seen in Figure 3. Figure 3

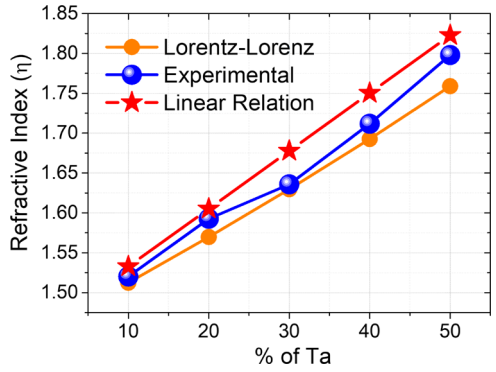

Figure 3. Experimental refractive index values as a function of the tantalum amount in comparison to the theoretical refractive index values based on Lorentz–Lorenz and linear equations.

corroborates the discussion on the densification of materials and exhibits an important refractive index variation curve with the concentration of tantalum, which can be applied for the design of multi- or monomodal waveguides. Depending on the thickness of the planar waveguides, this curve will be the basis for projecting guides from the precursor solutions of alkoxides. As previously reported, the sol–gel methodology employed has the great advantage of obtaining a large range of composition, which may not be possible through other chemical processes. Moreover, it has been observed that the major problem of residual silanol groups can be overcome with Ta_2O_5 addition, or even with the appropriate heat treatment, without loss of optical quality.

Similarities were observed in sol–gel-prepared SiO_2–Nb_2O_5 nanocomposite films,[21] which have also been described to exhibit refractive indexes in accordance with this model after achievement of full densification. In the literature, it has been also found a linear dependence of the refractive index on the molar fraction of the components of SiO_2–Ta_2O_5 films prepared by rf sputtering.[36,37] The linear dependence of the refractive index values on the calculated Ta_2O_5 molar fraction is also plotted in Figure 3 for comparison; however, the experimental data are closer to those calculated by the Lorentz–Lorenz equation, as described before.

An increase in the concentration of tantalum also influences the thickness of the films, as observed from Table 1. Layer thickness increased with increasing tantalum content from 10 to 50 mol %, namely, from 1.3 up to 2.0 μm (Table 1). A similar effect was also observed by Aquino et al.[35] in sol–gel-prepared SiO_2–Nb_2O_5 nanocomposite films. Gonçalves et al.[15,17] have also observed in the $70SiO_2$–$30HfO_2$ films doped with 0.3, 0.5, and 1 mol % of Er^{3+} ions that the viscosity of the initial solution was influenced by Er^{3+} concentration and consequently affected the thickness of each layer during preparation of the films, resulting in different final thicknesses. The metal ions (as Er^{3+} or Nb^{5+} and Ta^{5+}) added to the host exhibited a higher coordination number in comparison to Si^{2+}. Adding to this fact, the high reactivity of tantalum alkoxide

https://doi.org/10.1021/acsomega.0c05351
ACS Omega 2021, 6, 8784–8796

promotes the formation of cross-linking, with Si−O−M bonds, involving the monomers and polymers of the silicon oxide precursor in an acidic medium. Consequently, an increase of viscosity directly influences the thickness of films deposited on SiO_2−Si substrates.

Furthermore, it is observed an increase of refractive index values for all films after full densification compared with the films without any further annealing at 900 °C, attesting the removal of pores and structural defects. Measurements of the refractive index profile in TE and TM modes at 532 and 632.8 nm indicated that birefringence is practically negligible, even for higher tantalum contents. Low optical losses of around 0.8−1.0 dB/cm (±0.3) at 532 and 632.8 nm in the TE mode were measured for densified films containing up to 30 mol % Ta, demonstrating the high optical and structural quality of the films, which corroborates to the elimination of pores, any cracks, smooth surfaces, and host transparency. As reported before, the pores or phase separation can act as scattering centers, increasing the optical losses. A large number of scattering centers were observed in the case of films containing 60 and 50 mol % Ta, which can be explained by the phase separation increase, which will be discussed further using high-resolution transmission electron microscopy (HRTEM). The propagation loss values observed in the films containing up to 30 mol % Ta were low enough to consider these materials suitable for optical planar waveguides in photonic applications.

Figure 4 shows the $n(k)$ dispersion curves for the $(100 - x)SiO_2 - xTa_2O_5$ planar waveguides in the TE mode. The

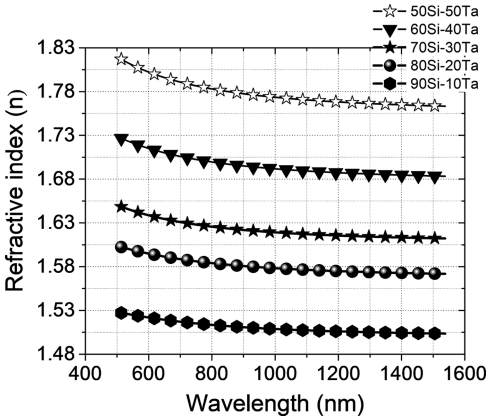

Figure 4. Dispersion curves of the planar waveguides based on Er^{3+}-doped SiO_2−Ta_2O_5 deposited onto the 10 μm SiO_2−Si (100) p-type silicon substrate with Si/Ta ratios of 90:10, 80:20, 70:30, 60:40, and 50:50.

refractive index (n) values obtained by the prism coupling technique, exhibited in Table 1, were used to construct the dispersion curves using the Cauchy equation.[35,38] Cauchy dispersion fitted properly shows a decrease in the refractive index values as a function of the wavelength in the visible and near-infrared spectral regions.

Figure 5 depicts the squared electric field (E^2) profiles for the TE_0 modes of the waveguides, which were calculated at 532, 632.8, and 1538 nm using the thickness and refractive index of the film, propagation angle, and effective refractive index for the Er^{3+}-doped SiO_2−Ta_2O_5 films deposited onto the 10 μm SiO_2−Si (100) p-type silicon substrate with Si/Ta ratios of (A) 90:10, (B) 80:20, (C) 70:30, (D) 60:40, and (E) 50:50. The confinement coefficients were calculated by the integrated intensity ratio, i.e., the ratio between the field intensity in the guiding film and the total intensity, which also includes the squared evanescent field based on the works reported by Aquino et al.[35] and Tosello et al.[39] Table 2 summarizes the confinement coefficients at 532, 632.8, and 1538 nm for TE_0 (transversal electric) mode. Confinement coefficients higher than 97% were observed for most planar waveguides, except for the films containing 10 and 20 mol %, which exhibited confinement coefficients of 66 and 72% at 1538 nm, respectively. The confinement coefficient of light for the planar waveguides demonstrated efficient light injection at 1538 nm, attesting that a well-confined mode at 1538 nm was obtained for application in the C-telecom band.

Figure 6 illustrates the FTIR spectra of the films with Si/Ta molar ratios from 10 to 50 mol % Ta deposited on Si (100) substrates. It is important to highlight here the use of films deposited directly on the silicon substrates, avoiding the thick layer of silica that would prevent the analysis of films up to 2 μm. Vibrational spectroscopy is an important technique for elucidating structural information relevant to the design of planar waveguides. As reported before by us,[20] the multilayer deposition process combined with the thermal treatment to eliminate organic and hydroxyl groups can be accompanied by the FTIR technique, which provides relevant structural information for design optical films. Thinner films were used in a previous study to monitor the film densification change with the annealing time.[20] FTIR was used as a fundamental complementary technique for refractive index measurements aiming to detect the elimination of water molecules and hydroxyl groups as the pores were closed densifying the film. Herein, thicker films of around 1.3−2.0 μm were analyzed. The thickness of the films is high enough to promote the appearance of interference fringes, which were clearly observed as a low-intensity interference fringe pattern from 4000 to near 1450 cm^{-1}. Due to the high thickness of the films, a cutoff in the 1245−1019 cm^{-1} range occurred, attributed to the most intense bands assigned to silica materials, indicating SiO_2 network formation. Usually, silica shows a band localized at around 1100 cm^{-1}, assigned to asymmetric stretching of Si−O−Si, and a shoulder located in the vicinity of 1200 cm^{-1}, which is more intense in porous materials.[35] The main focus of this work is to analyze the region below 1000 cm^{-1}, attributing the presence of Si−O−Si, Si−OH, and Si−Ta−Si vibrational modes, as well as phase separation through vibrational modes corresponding to Ta_2O_5 nanocrystals.

In addition to the Si−O−Si vibrational modes at 460 and 800 cm^{-1}, a band positioned at around 950 cm^{-1} is clearly observed, which is assigned to the Si−O−Ta or Si−OH stretching bond. As reported before, in accordance with Ferrari et al.,[20] after 15 min of annealing at 900 °C, H_2O was removed from the films with the lowest Ta concentrations. Here, longer annealing times were used to achieve constant values of the refractive index. Besides, the relative intensity of the absorption band at 950 cm^{-1} increased with the tantalum concentration, and consequently, it could be concluded that the band localized at around 950 cm^{-1} is assigned only to Si−O−Ta. This is evidence of the cross-linked structure with formation of a covalent bond between SiO_2 and Ta_2O_5.

The bands localized between 855 and 588 cm^{-1} are assigned to the Ta_2O_5 phonons, in agreement with the data reported by Huang and Chu.[40] A broadband emission in this spectral region appears, which is characteristic of Ta_2O_5 in the orthorhombic phase. A higher Ta content and the augmented

https://doi.org/10.1021/acsomega.0c05351
ACS Omega 2021, 6, 8784−8796

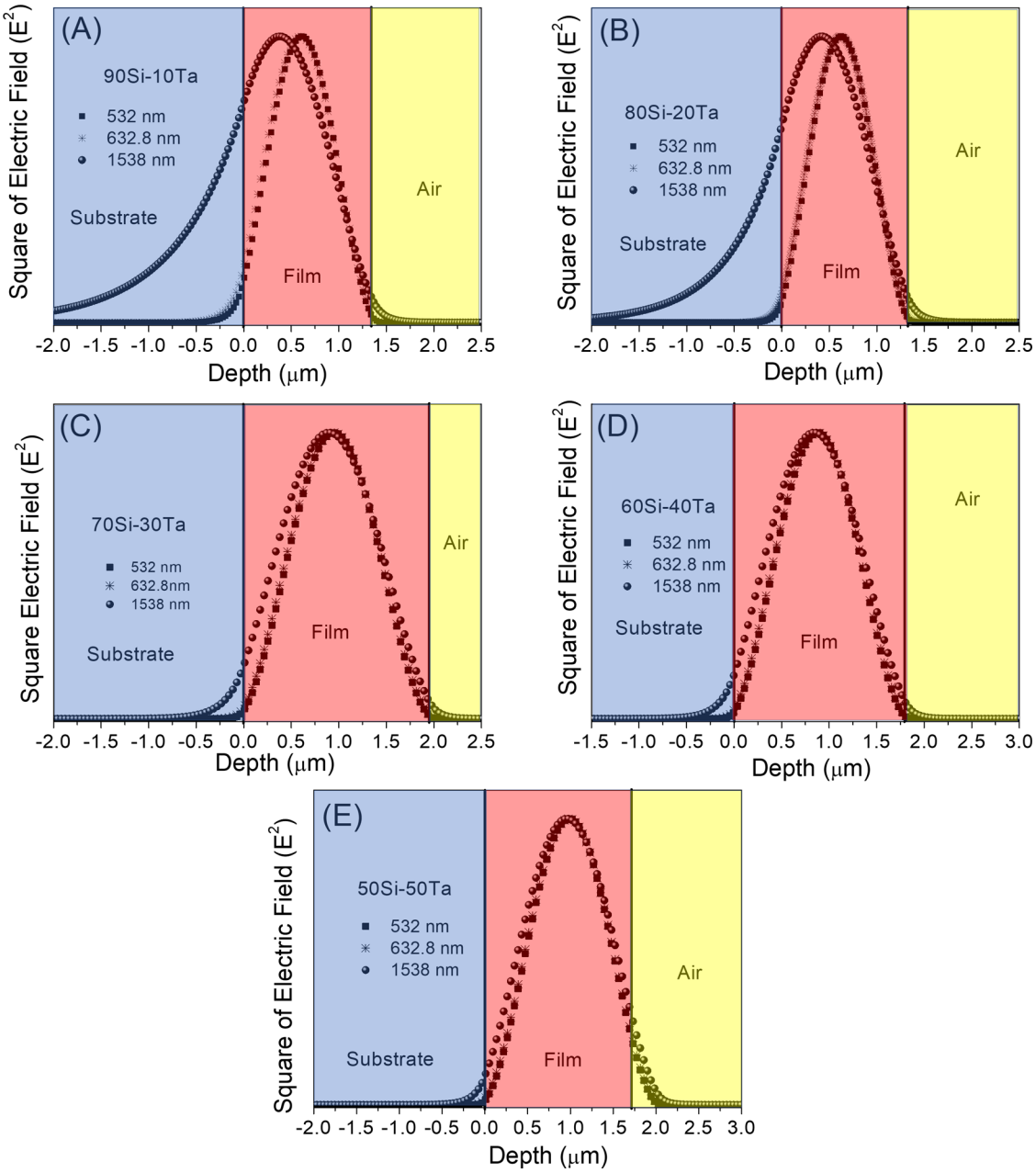

Figure 5. Squared electric field profiles in the TE_0 mode at 532, 632.8, and 1538 nm of the planar waveguides based on the Er^{3+}-doped SiO_2–Ta_2O_5 deposited onto 10 μm SiO_2–Si (100) p-type silicon substrate with Si/Ta ratios of (A) 90:10, (B) 80:20, (C) 70:30, (D) 60:40, and (E) 50:50.

Table 2. Percentage of the Confinement Coefficient of Light in Different Wavelengths for Planar Waveguides with Different Si/Ta Ratios

	wavelengths		
planar waveguide composition (Si/Ta)	532 nm	632.8 nm	1538 nm
90:10	97.96	96.72	65.98
80:10	99.42	98.94	72.06
70:30	99.77	99.68	96.81
60:40	99.86	99.77	97.04
50:50	97.41	97.11	94.51

relative intensity bands at around 855–588 cm^{-1} indicate the presence of phase separation, which is more evident for higher tantalum oxide concentrations.

The surface morphology of films was determined by AFM analysis, and the surface morphology and roughness in the 3 × 3 μm area are shown in Figure 7. Surface roughness is considered as one of the sources of losses, involving light interaction at the air–film interface. Depending on the roughness, diffuse scattering and consequently high propagation losses can be observed. However, considering a planar waveguide with high surface quality and low roughness, the respective losses are negligible. Homogeneous and crack-free films were obtained for all the compositions. Films do not exhibit any texture under AFM inspection. The AFM images display low surface roughness, with values of about 0.4 nm (±0.1). The losses are not correlated to the tantalum content, as already seen in similar waveguides based on silica–titania,[41] silica–hafnia,[16,17,42] and silica–zirconia.[19,43] Huong et al.[44]

https://doi.org/10.1021/acsomega.0c05351
ACS Omega 2021, 6, 8784–8796

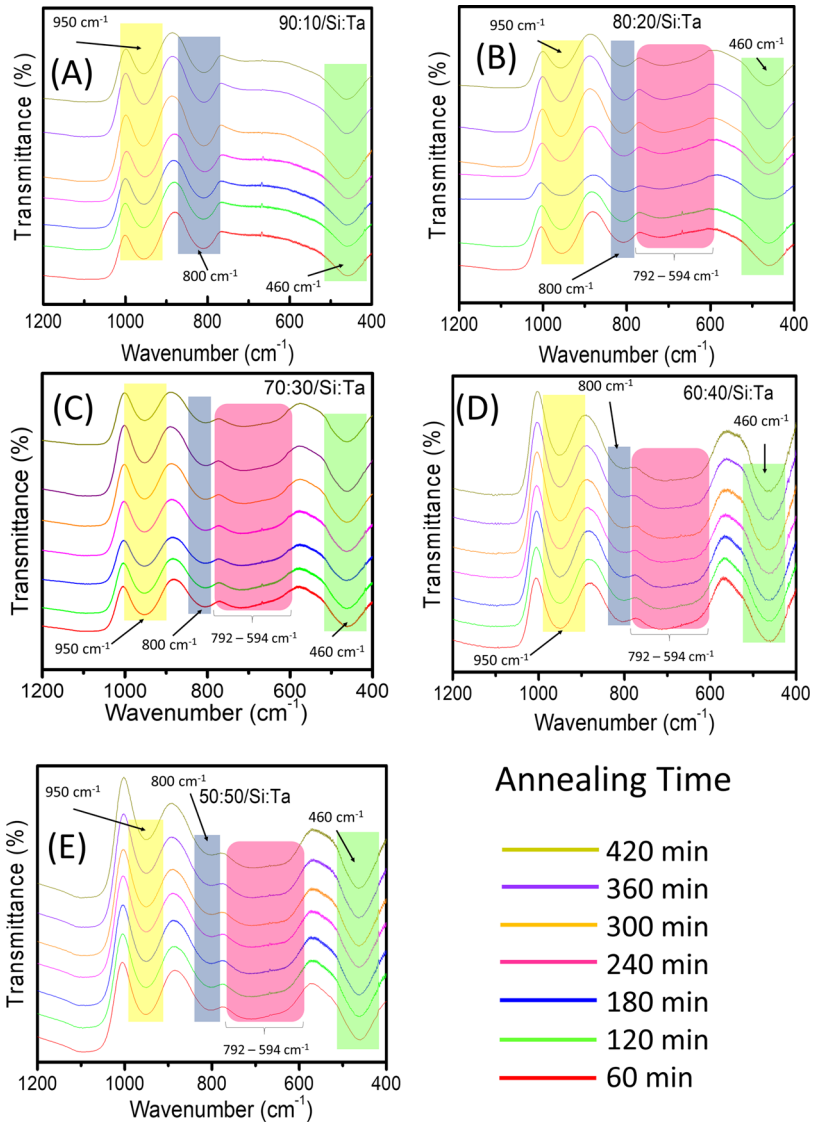

Figure 6. FTIR transmission spectra of Er^{3+}-doped SiO_2−Ta_2O_5 deposited onto the 10 μm SiO_2−Si (100) p-type silicon substrate with Si and Ta ratios of (A) 90:10, (B) 80:20, (C) 70:30, (D) 60:40, and (E) 50:50.

reported that planar waveguide based on silica−zirconia−alumina-doped Er^{3+} shows propagation loss <2.5 dB/cm with a surface roughness of 2 nm. Here, lower values of the surface roughness were obtained, attesting the high optical quality of the films.

Figure 8 shows the high-resolution transmission electron microscopy (HRTEM) images of the films after full densification. The ordered regions of dark contrast, which correspond to the nucleation and crystallization of Ta_2O_5 nanocrystals, have size distributions, in general, below 15 nm embedded into a SiO_2-based host. Nanocrystals embedded in an amorphous phase, with average sizes of around 2, 5, 7, and 8 nm for Er^{3+}-doped planar waveguide fully densified with Si/Ta ratios of (A) 90:10, (B) 80:20, (C) 70:30, and (D) 60:40, respectively, can be observed. The dependence of Ta_2O_5 nanoparticle size distribution on annealing temperature is remarkable. Planar waveguides require hosts with homogeneously dispersed nanoparticles and sizes on the order of λ^{-4} to avoid Rayleigh scattering. Electron scattering patterns (insets of Figure 8C and D) show that the nanoparticles are crystalline. In accordance with Stephenson and Roth in 1971,[45] Ta_2O_5 with an orthorhombic structure and with a = 6.19800 Å, b = 40.29000 Å, c = 3.88800 Å, $\alpha = \beta = \delta = 90°$, belonging to space group $P2_12_12$ in accordance with JCPDS 25-0922, can be represented by a chain of 8 edge-sharing pentagons, where each unit cell contains 22 Ta atoms and 55 O atoms, resulting at least in 12 different symmetry sites of Ta^{5+} ions. Consequently, this type of structure promotes the formation of numerous interstices with a volume able to accommodate several ions into its structure. Ferrari et al.[30] have reported the formation of nanocomposites based on Er^{3+}-doped SiO_2−Ta_2O_5 prepared by the sol−gel method, in which orthorhombic Ta_2O_5 nanocrystals were grown in accordance with the same crystalline structure reported by Stephenson and Roth in 1971.[45]

Figure 9 shows the excitation spectra of the Er^{3+}-doped SiO_2−Ta_2O_5 planar waveguides with fixed emission at 1528 nm. The excitation spectra show bands that are assigned to the intraconfigurational f−f transition of Er^{3+} ions. There are observed bands localized at around 378 and 521 nm assigned to $^4I_{15/2} \rightarrow {}^4G_{11/2}$ and $^4I_{15/2} \rightarrow {}^2H_{11/2}$, respectively, and a band below 325 nm with a maximum between 278 and 271 nm, in

https://doi.org/10.1021/acsomega.0c05351
ACS Omega 2021, 6, 8784−8796

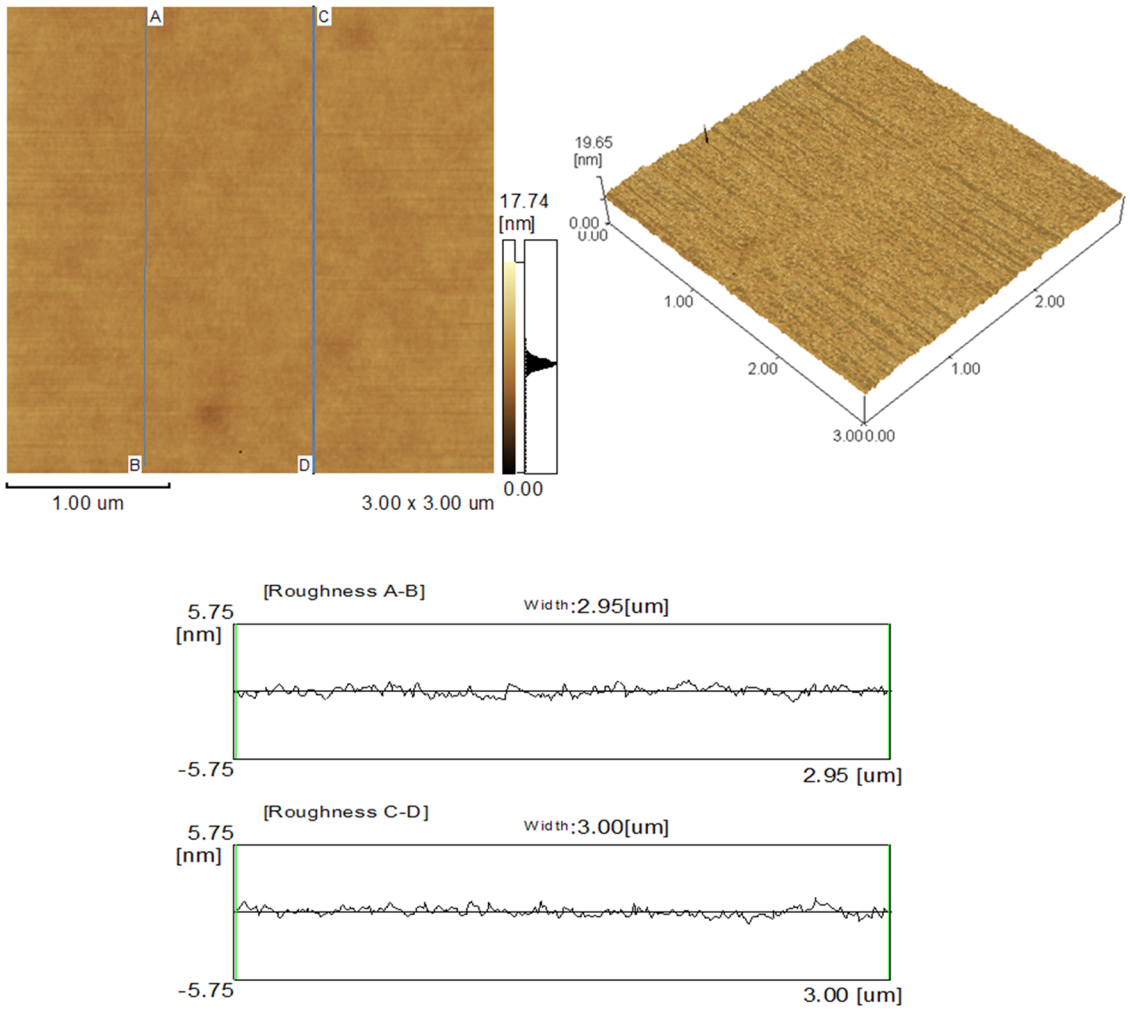

Figure 7. Two-dimensional (2D), three-dimensional (3D), and roughness profile of the Er^{3+}- doped SiO_2−Ta_2O_5 film after full densification at 900 °C.

which the maximum of the band varies according to the amount Ta, can be attributed to the charge transfer between oxygen and the rare-earth metal. It is clearly seen that the intensity of the bands assigned to the f−f transitions increases as a function of the amount of Ta present in the system. It was discussed previously that the increase of nanoparticle size is dependent on the higher Ta amount, and it can be assumed the preferential distribution of Er^{3+} ions in a Ta_2O_5 crystalline environment, as reported before.[30]

Figure 10 shows the emission spectra of the planar waveguides in the region between 1400 and 1700 nm, when excited at 271, 274, and 278 nm for samples with Si/Ta ratio of 80:20, 70:30, and 50:50. This emission band is attributed to the $^4I_{13/2} \rightarrow {}^4I_{15/2}$ f−f intraconfigurational transition of the Er^{3+} ion. This band has an intense photoluminescence emission in the third telecommunication window region, with a FWHM between 50 and 62 nm, whose spectral bandwidth changes slightly with the content of tantalum oxide. In this work, a temperature of 900 °C was used to maintain the average size of nanoparticles, with a narrow size distribution, lower than 10 nm. Table 3 shows the FWHM values obtained in this work in comparison with other planar waveguides reported in the literature. It can be observed similar or even higher FWHM values in comparison with other waveguides reported in the literature, indicating interesting results for applications in devices that require broadband emission at 1550 nm.

Similar compounds (powders) exhibited a broader bandwidth, which increased from 74 up to 93 nm as the tantalum oxide content increased for samples annealed at 1100 °C for 2 h. This inhomogeneous broadening is related to the presence of Er^{3+} ions preferentially in many different sites in the orthorhombic Ta_2O_5 structure. As mentioned before, orthorhombic Ta_2O_5 has a huge unit cell with 12 sites occupied by Ta^{5+} ions, so if the Er^{3+} ions substitute the Ta^{5+} ions, the observed inhomogeneous broadening in the emission spectra can be explained. The significant meaning of broad bandwidth values is related to the presence of a more flat-gain region in Er^{3+}-doped materials for amplifiers to be combined to wavelength division multiplexing (WDM). The large optical bandwidth of the Er^{3+}-doped SiO_2−Ta_2O_5 waveguides prepared by the sol−gel method makes them a suitable candidate for WDM applications.

4. CONCLUSIONS

Er^{3+}-doped planar waveguides based on SiO_2−Ta_2O_5 deposited onto SiO_2−Si and Si (100) substrates were prepared successfully by the sol−gel process followed by the dip-coating technique. This set of techniques for preparation allowed obtaining planar waveguides with suitable optical properties for

https://doi.org/10.1021/acsomega.0c05351
ACS Omega 2021, 6, 8784−8796

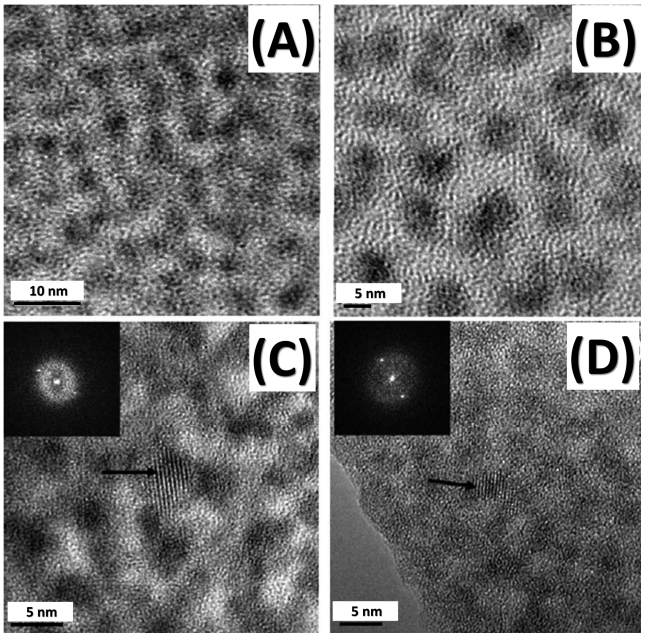

Figure 8. HRTEM micrographs of the Er^{3+}-doped planar waveguides fully densified at 900 °C with Si/Ta ratios of (A) 90:10, (B) 80:20, (C) 70:30, and (D) 60:40.

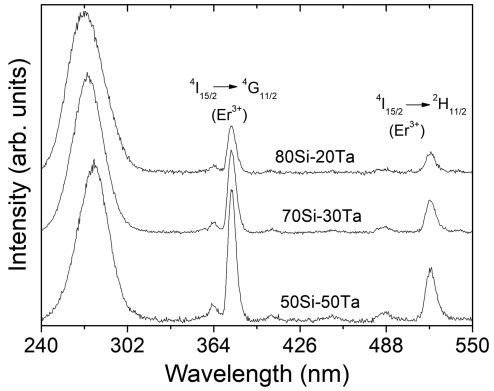

Figure 9. Excitation spectra of the Er^{3+}-doped SiO_2–Ta_2O_5 planar waveguides with fixed emission at 1528 nm.

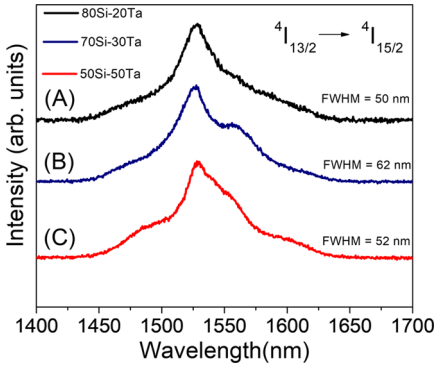

Figure 10. Photoluminescence spectra assigned to the $^4I_{13/2} \rightarrow {}^4I_{15/2}$ transition of the Er^{3+} ions for the planar waveguides based on Er^{3+}-doped SiO_2–Ta_2O_5 deposited onto the 10 μm SiO_2–Si (100) p-type silicon substrate with Si/Ta ratios of (A) 90:10, (B) 70:30, and (C) 50:50.

Table 3. FWHM Values of $^4I_{13/2} \rightarrow {}^4I_{15/2}$ Emission around 1550 nm Assigned to the Er^{3+}-Doped Planar Waveguides from Different Compositions

planar waveguides composition	FWHM (nm)	references
SiO_2–Ta_2O_5	between 50 and 62	results of this work
SiO_2–Nb_2O_5	between 48 and 52	35
SiO_2–HfO_2	48	42
SiO_2–TiO_2	between 45 and 51	18

applications in optical devices. The annealing temperature, 900 °C, at different times, has been shown to be enough to promote the densification, pore elimination, and increase and control the refractive index values. The refractive index also has been shown to be dependent on the Ta concentration and annealing time. The surface of the planar waveguides displays low roughness, of around 0.245 and 0.436 nm, and contributes to low loss in waveguides by means of scattering. An average attenuation coefficient of 1 dB/cm at 514.5 and 612.8 nm was verified. Confinement of light in three wavelengths (532, 632.8, and 1538 nm) of above 65% in the planar waveguides also contributes to the reduction of optical loss of light propagation. The efficiency of confinement of light inside the planar waveguides appeared to be dependent on the amount of Ta present in the system. The excitation spectra showed characteristic bands assigned to the intraconfigurational f–f transition of Er^{3+} ions and a band below 300 nm assigned to the charge transfer between Er^{3+} and O^{2-} ions when fixing the emission at 1538 nm. The planar waveguides showed intense emission in the region between 1440 and 1700 nm (C-telecom band) with an intensity maximum at approximately 1538 nm and a FWHM of the emission band between 50 and 60 nm. Based on the information obtained in this work, the synergism between optical, structural, surface, and photoluminescent properties brings together important characteristics that make this system a potential device for application in integrated circuits and for use in optical amplification at 1550 nm, photodectors, and devices for augmented reality.

AUTHOR INFORMATION

Corresponding Author

Rogéria R. Gonçalves − *Laboratório de Materiais Luminescentes Micro e Nanoestruturados−Mater Lumen, Departamento de Química, FFCLRP, Universidade de São Paulo, 14040-900 São Paulo, Brazil;* orcid.org/0000-0001-5540-7690; Phone: +55 16 36024851; Email: rrgoncalves@ffclrp.usp.br; Fax: +55 16 363288151

Authors

Jefferson L. Ferrari − *Laboratório de Materiais Luminescentes Micro e Nanoestruturados−Mater Lumen, Departamento de Química, FFCLRP, Universidade de São Paulo, 14040-900 São Paulo, Brazil; Desenvolvimento de Materiais Inorgânicos com Terras Raras−DeMITeR, Laboratório de Materiais Fotoluminescentes (LAMAF), Instituto de Química−(IQ), Universidade Federal de Uberlândia−(UFU), 38400-902 Uberlândia, Minas Gerais, Brazil*

Karmel de O. Lima − *Laboratório de Materiais Luminescentes Micro e Nanoestruturados−Mater Lumen, Departamento de Química, FFCLRP, Universidade de São Paulo, 14040-900 São Paulo, Brazil*

Complete contact information is available at:

https://doi.org/10.1021/acsomega.0c05351
ACS Omega 2021, 6, 8784−8796

https://pubs.acs.org/10.1021/acsomega.0c05351

Notes

The authors declare no competing financial interest.

■ ACKNOWLEDGMENTS

The authors thank FAPESP (2020/05319-9, 2018/18213-4), CNPq, and CAPES. This work has been supported by the Brazilian Synchrotron Light Laboratory (LNLS) under proposal TEM-HR 7952. This study was financed in part by the Coordenação de Aperfeiçoamento de Pessoal de Nível Superior—Brasil (CAPES)—Finance Code 001.

■ REFERENCES

(1) Sohler, W.; De La Rue, R. Integrated Optics - New Material Platforms, Devices and Applications. *Laser Photonics Rev.* **2012**, *6*, A21−A22.
(2) Yebo, N. A.; Lommens, P.; Hens, Z.; Baets, R. An Integrated Optic Ethanol Vapor Sensor Based on a Silicon-on-Insulator Microring Resonator Coated with a Porous ZnO Film. *Opt. Express* **2010**, *18*, 11859.
(3) Fuentes, O.; Del Villar, I.; Corres, J. M.; Matias, I. R. Lossy Mode Resonance Sensors Based on Lateral Light Incidence in Nanocoated Planar Waveguides. *Sci. Rep.* **2019**, *9*, No. 8882.
(4) Liu, L.; Zhou, X.; Wilkinson, J. S.; Hua, P.; Song, B.; Shi, H. Integrated Optical Waveguide-Based Fluorescent Immunosensor for Fast and Sensitive Detection of Microcystin-LR in Lakes: Optimization and Analysis. *Sci. Rep.* **2017**, *7*, No. 3655.
(5) Li, L.; Nie, W.; Li, Z.; Lu, Q.; Romero, C.; Vázquez De Aldana, J. R.; Chen, F. All-Laser-Micromachining of Ridge Waveguides in LiNbO3 Crystal for Mid-Infrared Band Applications. *Sci. Rep.* **2017**, *7*, No. 7034.
(6) Zhang, W.; Wang, Z.; Xu, J. Research on a Surface-Relief Optical Waveguide Augmented Reality Display Device. *Appl. Opt.* **2018**, *57*, 3720.
(7) Zhang, Y.; Fang, F. Development of Planar Diffractive Waveguides in Optical See-through Head-Mounted Displays. *Precis. Eng.* **2019**, *60*, 482−496.
(8) Lee, Y.-H.; Zhan, T.; Wu, S.-T. Prospects and Challenges in Augmented Reality Displays. *Virtual Reality Intell. Hardware* **2019**, *1*, 10−20.
(9) Eisen, L.; Meyklyar, M.; Golub, M.; Friesem, A. A.; Gurwich, I.; Weiss, V. Planar Configuration for Image Projection. *Appl. Opt.* **2006**, *45*, 4005.
(10) Šimurka, L.; Čtvrtlík, R.; Tomaštík, J.; Bektaş, G.; Svoboda, J.; Bange, K. Mechanical and Optical Properties of SiO2 Thin Films Deposited on Glass. *Chem. Pap.* **2018**, *72*, 2143−2151.
(11) Mears, R. J.; Reekie, L.; Jauncey, I. M.; Payne, D. N. Low-Noise Erbium-Doped Fibre Amplifier Operating at 1.54μm. *Electron. Lett.* **1987**, *23*, 1026.
(12) Desurvire, E.; Simpson, J. R.; Becker, P. C. High-Gain Erbium-Doped Traveling-Wave Fiber Amplifier. *Opt. Lett.* **1987**, *12*, 888.
(13) Laming, R. I.; Farries, M. C.; Morkel, P. R.; Reekie, L.; Payne, D. N.; Scrivener, P. L.; Fontana, F.; Righetti, A. Efficient Pump Wavelengths of Erbium-Doped Fibre Optical Amplifier. *Electron. Lett.* **1989**, *25*, 12−14.
(14) Righini, G. C.; Berneschi, S.; Nunzi Conti, G.; Pelli, S.; Moser, E.; Retoux, R.; Féron, P.; Gonçalves, R. R.; Speranza, G.; Jestin, Y.; Ferrari, M.; Chiasera, A.; Chiappini, A.; Armellini, C. Er3+-Doped Silica-Hafnia Films for Optical Waveguides and Spherical Resonators. *J. Non-Cryst. Solids* **2009**, *355*, 1853−1860.
(15) Gonçalves, R. R.; Carturan, G.; Zampedri, L.; Ferrari, M.; Montagna, M.; Chiasera, A.; Righini, G. C.; Pelli, S.; Ribeiro, S. J. L.; Messaddeq, Y. Sol-Gel Er-Doped SiO2-HfO2 Planar Waveguides: A Viable System for 1.5 Mm Application. *Appl. Phys. Lett.* **2002**, *81*, 28−30.
(16) Gonçalves, R. R.; Carturan, G.; Zampedri, L.; Ferrari, M.; Chiasera, A.; Montagna, M.; Righini, G. C.; Pelli, S.; Ribeiro, S. J. L.; Messaddeq, Y. Infrared-to-Visible CW Frequency Upconversion in Erbium Activated Silica-Hafnia Waveguides Prepared by Sol-Gel Route. *J. Non-Cryst. Solids* **2003**, *322*, 306−310.
(17) Gonçalves, R. R.; Carturan, G.; Montagna, M.; Ferrari, M.; Zampedri, L.; Pelli, S.; Righini, G. C.; Ribeiro, S. J. L.; Messaddeq, Y. Erbium-Activated HfO2-Based Waveguides for Photonics. *Opt. Mater.* **2004**, *25*, 131−139.
(18) Zampedri, L.; Ferrari, M.; Armellini, C.; Visintainer, F.; Tosello, C.; Ronchin, S.; Rolli, R.; Montagna, M.; Chiasera, A.; Pelli, S.; Righini, G. C.; Monteil, A.; Duverger, C.; Gonçalves, R. R. Erbium-Activated Silica-Titania Planar Waveguides. *J. Sol-Gel Sci. Technol.* **2003**, *26*, 1033−1036.
(19) Gonçalves, R. R.; Guimarães, J. J.; Ferrari, J. L.; Maia, L. J. Q.; Ribeiro, S. J. L. Active Planar Waveguides Based on Sol-Gel Er3+-Doped SiO2-ZrO2 for Photonic Applications: Morphological, Structural and Optical Properties. *J. Non-Cryst. Solids* **2008**, *354*, 4846−4851.
(20) Ferrari, J. L.; Lima, K. O.; Maia, L. J. Q.; Gonçalves, R. R. Sol-Gel Preparation of near-Infrared Broadband Emitting Er 3+-Doped SiO2-Ta2O5 Nanocomposite Films. *Thin Solid Films* **2010**, *519*, 1319−1324.
(21) Aquino, F. T.; Caixeta, F. J.; de Oliveira Lima, K.; Kochanowicz, M.; Dorosz, D.; Gonçalves, R. R. Broadband NIR Emission from Rare Earth Doped-SiO2-Nb2O5 and SiO2-Ta2O5 Nanocomposites. *J. Lumin.* **2018**, *199*, 138−142.
(22) Aquino, F. T.; Pereira, R. R.; Ferrari, J. L.; Ribeiro, S. J. L.; Ferrier, A.; Goldner, P.; Gonçalves, R. R. Unusual Broadening of the NIR Luminescence of Er3+-Doped Nb 2O5 Nanocrystals Embedded in Silica Host: Preparation and Their Structural and Spectroscopic Study for Photonics Applications. *Mater. Chem. Phys.* **2014**, *147*, 751−760.
(23) Ferrari, J. L.; Lima, K. O.; Maia, L. J. Q.; Ribeiro, S. J. L.; Gomes, A. S. L.; Gonçalves, R. R. Broadband NIR Emission in Sol-Gel Er 3-Activated SiO 2-Ta 2O 5 Glass Ceramic Planar and Channel Waveguides for Optical Application. *J. Nanosci. Nanotechnol.* **2011**, *11*, 2540−2544.
(24) Zha, J.; Roggendorf, H. Sol-Gel Science, the Physics and Chemistry of Sol-Gel Processing, Ed. by C. J. Brinker and G. W. Scherer, Academic Press, Boston 1990, Xiv, 908 Pp., Bound?ISBN 0-12-134970-5. *Adv. Mater.* **1991**, *3*, 522.
(25) Jung-Chieh Su, H.-C.; Chien-Kang Kao, H.-T. I.-N.; Lin, H.-C. C.-H. T.; Chi, H.-C. C.-C.; Hsin-Chu; Yung-Sheng Liu, H.-C. Manufacturing Process for Preparing Sol-Gel Optical Waveguides. U.S. Patent US6.391,515B12002.
(26) Ferrari, J. L.; Lima, K. O.; Maia, L. J. Q.; Gonçalves, R. R. Sol-Gel Preparation of near-Infrared Broadband Emitting Er3+-Doped SiO2-Ta2O5 Nanocomposite Films. *Thin Solid Films* **2010**, *519*, 1319−1324.
(27) Ferrari, J. L.; Lima, K. O.; Maia, L. J. Q.; Ribeiro, S. J. L.; Gonaçalves, R. R. Structural and Spectroscopic Properties of Luminescent Er 3+-Doped SiO2-Ta2O5 Nanocomposites. *J. Am. Ceram. Soc.* **2011**, *94*, 1230−1237.
(28) Ferrari, J. L.; Lima, K. O.; Maia, L. J. Q.; Ribeiro, S. J. L.; Gomes, A. S. L.; Gonçalves, R. R. Broadband NIR Emission in Sol-Gel Er3+-Activated SiO2-Ta2O5 Glass Ceramic Planar and Channel Waveguides for Optical Application. *J. Nanosci. Nanotechnol.* **2011**, *11*, 2540−2544.
(29) Yoldas, B. E. Investigations of Porous Oxides as an Antireflective Coating for Glass Surfaces. *Appl. Opt.* **1980**, *19*, 1425.
(30) Ferrari, J. L.; Lima, K. O.; Maia, L. J. Q.; Ribeiro, S. J. L.; Goncalves, R. R. Structural and Spectroscopic Properties of Luminescent Er3+-Doped SiO2-Ta2O5 Nanocomposites. *J. Am. Ceram. Soc.* **2011**, *94*, 1230−1237.
(31) Montagna, M.; Chiasera, A.; Moser, E.; Visintainer, F.; Ferrari, M.; Zampedri, L.; Gonçalves, R. R.; Ribeiro, S. J. L.; Martucci, A.; Guglielmi, M.; Ivanda, M.; Almeida, R. M. Nucleation and Crystallization of Titania Nanoparticles in Silica Titania Planar

Waveguides: A Study by Low Frequency Raman Scattering. *Mater. Sci. Forum* **2004**, *455−456*, 520−526.
(32) Zampedri, L.; Mattarelli, M.; Montagna, M.; Gonçalves, R. R. Evaluation of Local Field Effect on the I 13 2 4 Lifetimes in Er-Doped Silica-Hafnia Planar Waveguides. *Phys. Rev. B* **2007**, *75*, No. 073105.
(33) Chaneliere, C.; Autran, J. L.; Devine, R. A. B.; Balland, B. Tantalum Pentoxide (Ta2O5) Thin Films for Advanced Dielectric Applications. *Mater. Sci. Eng., R* **1998**, *22*, 269−322.
(34) Rocha, L. A.; Schiavon, M. A.; Ribeiro, S. J. L.; Gonçalves, R. R.; Ferrari, J. L. Eu3+-Doped SiO2−Gd2O3 Prepared by the Sol−Gel Process: Structural and Optical Properties. *J. Sol-Gel Sci. Technol.* **2015**, *76*, 260−270.
(35) Aquino, F. T.; Ferrari, J. L.; Ribeiro, S. J. L.; Ferrier, A.; Goldner, P.; Gonçalves, R. R. Broadband NIR Emission in Novel Sol-Gel Er3+-Doped SiO 2-Nb2O5 Glass Ceramic Planar Waveguides for Photonic Applications. *Opt. Mater.* **2013**, *35*, 387−396.
(36) Cevro, M. Ion-Beam Sputtering of (Ta2O5)x- (SiO2)1-x Composite Thin Films. *Thin Solid Films* **1995**, *258*, 91−103.
(37) Kobayashi, M.; Terui, H. Refractive Index and Attenuation Characteristics of SiO_2−Ta_2O_5 Optical Waveguide Film. *Appl. Opt.* **1983**, *22*, 3121.
(38) Barbosa, A. J.; Dias Filho, F. A.; Messaddeq, Y.; Ribeiro, S. J. L.; Gonçalves, R. R.; Lüthi, S. R.; Gomes, A. S. L. 1.5μm Emission and Infrared-to-Visible Frequency Upconversion in Er+3/Yb+3-Doped Phosphoniobate Glasses. *J. Non-Cryst. Solids* **2006**, *352*, 3636−3641.
(39) Tosello, C.; Rossi, F.; Ronchin, S.; Rolli, R.; Righini, G.; Pozzi, F.; Pelli, S.; Fossi, M.; Moser, E.; Montagna, M.; Ferrari, M.; Duverger, C.; Chiappini, A.; De Bernardi, C. Erbium-Activated Silica−Titania Planar Waveguides on Silica-on-Silicon Substrates Prepared by Rf Sputtering. *J. Non-Cryst. Solids Solids* **2001**, *284*, 230−236.
(40) Huang, A. P.; Chu, P. K. Crystallization Improvement of Ta2O5 Thin Films by the Addition of Water Vapor. *J. Cryst. Growth* **2005**, *274*, 73−77.
(41) Chiasera, A.; Tosello, C.; Moser, E.; Montagna, M.; Belli, R.; Gonçalves, R. R.; Righini, G. C.; Pelli, S.; Chiappini, A.; Zampedri, L.; Ferrari, M. Er3+/Yb3+-Activated Silica−Titania Planar Waveguides for EDPWAs Fabricated by Rf-Sputtering. *J. Non-Cryst. Solids* **2003**, *322*, 289−294.
(42) Gonçalves, R. R.; Carturan, G.; Zampedri, L.; Ferrari, M.; Montagna, M.; Chiasera, A.; Righini, G. C.; Pelli, S.; Ribeiro, S. J. L.; Messaddeq, Y. Sol-Gel Er-Doped SiO2−HfO2 Planar Waveguides: A Viable System for 1.5 Mm Application. *Appl. Phys. Lett.* **2002**, *81*, 28−30.
(43) Cunha, C. D. S.; Ferrari, J. L.; De Oliveira, D. C.; Maia, L. J. Q.; Gomes, A. S. L.; Ribeiro, S. J. L.; Gonçalves, R. R. NIR Luminescent Er^{3+}/Yb^{3+}Co-Doped SiO<inf>2</Inf>-ZrO<inf>2</Inf>nanostructured Planar and Channel Waveguides: Optical and Structural Properties. *Mater. Chem. Phys.* **2012**, *136*, 120−129.
(44) Thu Huong, T.; Kim Anh, T.; Hoai Nam, M.; Barthou, C.; Strek, W.; Quoc Minh, L. Preparation and Infrared Emission of Silica−Zirconia−Alumina Doped with Erbium for Planar Waveguide. *J. Lumin.* **2007**, *122−123*, 911−913.
(45) Stephenson, N. C.; Roth, R. S. The Crystal Structure of the High Temperature Form of Ta2O5. *J. Solid State Chem.* **1971**, *3*, 145−153.

https://doi.org/10.1021/acsomega.0c05351
ACS Omega 2021, 6, 8784−8796